Chinese Chemical Letters 33 (2022) 4069–4073

Contents lists available at ScienceDirect

Chinese Chemical Letters

journal homepage: www.elsevier.com/locate/cclet

Structural landscape investigations on bendable plastic crystals of isonicotinamide polymorphs

Jianting Li[a], Jiaquan Li[a], Hongji Liu[a], Li Zhang[b,*], Yang Lu[b], Zhengzheng Zhou[a,*]

[a] NMPA Key Laboratory for Safety Evaluation of Cosmetics, Guangdong Provincial Key Laboratory of Tropical Disease Research, Department of Hygiene Inspection & Quarantine Science, School of Public Health, Southern Medical University, Guangzhou 510515, China
[b] Beijing City Key Laboratory of Polymorphic Drugs, Institute of Materia Medica, Chinese Academy of Medical Sciences and Peking Union Medical College, Beijing 100050, China

ARTICLE INFO

Article history:
Received 27 December 2021
Revised 21 March 2022
Accepted 21 March 2022
Available online 25 March 2022

Keywords:
Isonicotinamide
Polymorph
Plasticity
Slip plane
Bending crystal

ABSTRACT

Three polymorphs (forms **I**, **II** and **V**) of isonicotinamide (INA) were mechanically flexible and exhibited one-dimensional (1D) plasticity. Anisotropic intermolecular interactions contribute to the plasticity of single crystals: weak dispersive interactions between slip planes such as 1D columns in forms **I** and **II** or 2D layers in form **V** were stabilized by strong hydrogen bonds, allowing the layer or column's surface to glide smoothly without hindrance. The disparity of intermolecular interactions on plastic properties of INA polymorphic crystals was confirmed by energy framework analysis, nanoindentation tests and micro-Raman spectroscopy. The crystal which exhibits plastic property provides a promising application in pharmaceuticals and material sciences.

Organic crystals with plastic or elastic properties, a kind of advanced functional materials, are future prospects for optical waveguides [1], organic electronics [2], muscle-mimetic biomaterials [3], sensors [4], bioinspired natural fibers [5,6], fine chemicals [7], pharmaceutical industry and other fields [8–11]. It was first observed in hexachlorobenzene [12] and then other 16 bending crystals were explored by Reddy [13], which greatly enlarged the types of plastic bending crystals and proved the feasibility of finding new bending crystals. However, it should be noted that approximately >80% of organic compounds exist in different solid-state forms [14]. Different polymorphs demonstrate potential different physicochemical properties such as dissolution, solubility, *etc*., but mechanical differences on bendable single crystals lack further investigations [15–18]. At present, the mechanical behaviors of polymorphic compounds remained unexplored.

Isonicotinamide (INA) is a popular coformer extensively employed as a partner molecule with active pharmaceutical ingredients (APIs) in cocrystal preparation. It was generally recognized as safe (GRAS) and presented high water solubility [19–22]. So far, it has been reported that INA was capable of forming six polymorphs (Table S1 in Supporting information) [22]. Forms **I** [23] and **II** [24] are more easily obtained regardless of the solvent type and form **V** [27] occurred when the methyl group was presented. However, forms **III** [25] and **VI** [28] were always obtained from a cocrystal of API with INA, and form **IV** [26] was obtained only as a mixture with form **II**. Hence, forms **I**, **II** and **V** were selected and prepared in the present study. The three polymorphs exhibit 1D plasticity, which provides a model to explain the relationship between the types of intermolecular interactions in the crystal structure calculated by energy framework and the difference of plasticity examined by nanoindentation tests among polymorphs.

The cell parameters obtained from single crystal X-ray diffraction (SXRD) were found to be consistent with CIF documents deposited in Cambridge Crystallographic Data Center (CCDC), implying that single crystals of forms **I** (CSD refcode EHOWIH01) [23], **II** (CSD refcode EHOWIH02) [24] and **V** (CSD refcode EHOWIH05) [27] were successfully prepared (Table S2 in Supporting information). Single crystals of forms **I** and **II** both underwent irreversible plastic deformation when bent with a metal needle on (100)/(−100) faces with the largest area. Form **V** exhibits excellent plasticity when stress is applied on narrow faces (010)/(0−10) but not on the wider face (Fig. 1). All the polymorphs exhibit 1D plasticity and were directly folded in half without fracture, which was not allowed to be twisted [17].

In form **I** (space group P 21/c with a = 10.1756 (11) Å, b = 5.7319(6) Å, c = 10.034(1) Å, β = 98.169(1)°), N − H···O (2.93(3) Å) hydrogen-bonded dimers are interconnected along c axis by another N−H···O hydrogen-bonded dimer with NH_2 as donor

* Corresponding authors.
E-mail addresses: zhangl@imm.ac.cn (L. Zhang), zhouzz418@smu.edu.cn (Z. Zhou).

https://doi.org/10.1016/j.cclet.2022.03.090
1001-8417/

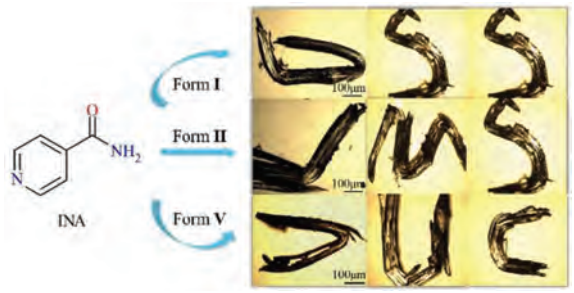

Fig. 1. Screenshots of irreversible plastic bending of INA forms **I, II** and **V** and deformed into special shapes.

and C=O as acceptor (2.93(3) Å) and expanded along *b* axis through N–H···O hydrogen-bonds and C–H···N weak interactions a centroid-to-centroid distance of 5.73 Å. This generates a stable column-like structure with two-independent tapes staggered in arrangement through strong hydrogen bonds (Fig. 2). Columns are formed parallel to (100) faces and extended through *a* axis with weaker interactions composed of C–H···N (between pyridine rings, 3.42(3) Å, 3.47(3) Å), resulting in some smooth slip planes between columns (Fig. S1 in Supporting information). When pressure is applied on (100) face, the internal columns slide along the *c* axis and exhibit excellent plasticity.

In form **II** (space group *P* 21/c with $a = 15.735(3)$ Å, $b = 7.9976(18)$ Å, $c = 9.885(3)$ Å, $\beta = 105.586(17)°$), molecules run along the *c* axis by N–H···O hydrogen bonds (2.95(2) Å) and C–H···O weak interactions (3.24(3) Å) and extend backward along *b* axis by N–H···N (between pyridine rings, 2.98(6) Å) hydrogen bonds and C–H···N (3.83(1) Å) weak interactions to form 2D tapes (Fig. 2). Besides, two-independent tapes staggered in arrangement to extend along *a* axis are derived from weak interactions C–H···C (3.52(3) Å; 3.41(3) Å) to form a column-like structure. These columns are parallel to (100) faces, with the same columnar structure exposed on both sides. As a result, slip planes are formed parallel to the wider (100) face of the crystals (Fig. S2 in Supporting information).

In form **V** (space group *P* 21/c with $a = 5.1923(11)$ Å, $b = 9.466(3)$ Å, $c = 12.259(3)$ Å, $\beta = 91.217(7)°$), molecules extend along the *b* axis by forming dimers of N–H···O(2.94(2) Å) hydrogen bonds and C–H···O (between the pyridine ring and the neighboring carbonyl groups: 3.35(2) Å) short contacts mediated dimers and run along *c* axis by interconnecting through N–H···N hydrogen-bonds (2.99(3) Å) to form a zigzag tape parallel to (102) plane (Fig. 2). Meanwhile, the tapes expand along *a* and *c* axes with weak interactions C–H···O(3.37(3) Å) to produce independent 2D layers parallel to (001) face. Therefore, the slip planes (011) are formed intersecting (001) faces at 52.32° (Fig. S3 in Supporting information).

1D plastically bendable crystals should have a slip plane as a prerequisite, and weakly interconnected molecular layers slide over other layers when mechanically stressed [15]. Three crystal forms of INA possess the same space group but exhibit different intermolecular interactions. Weak interactions such as C–H···N and C–H···C between rigid one-dimensional (1D) columns or chains in forms **I** and **II** and two-dimensional (2D) layers generated by moderately strong interactions such as C–H···O in form **V** are possible as long as the column's face is allowed to slip smoothly without obstruction [18,29].

The energy framework was used to calculate the interlayer and intralayer energy of slip plane identified by attachment energy (*E*att) (Table 1) [30–35]. The interlayer energy of sliding plane is always found less than the intralayer energy [29]. The (100) plane in INA form **I** is found to have the lowest attachment energy and corresponds to the largest surface in the predicted crystal morphology. The molecules within (100) plane are hydrogen-bonded (N–H···O, 2.93(3) Å), whereas weaker interactions C–H···N (3.42(3) Å; 3.47(3) Å) are present between these planes (Fig. S1). Therefore, the total interlayer interaction energy (−86.2 kJ/mol) is lower than the total intralayer interaction energies (−91.8 kJ/mol), indicating that the molecules slide along (100) plane is energetically favorable (Tables S3 and S4 and Fig. S4 in Supporting information). The molecules in slip plane (100) identified by *E*att in INA form **II** are interconnected through N–H···O hydrogen bonds (2.95(2) Å), while only weak contact C–H···C (3.52(3) Å, 3.41(3) Å) interacted between layers (Fig. S2). The significantly smaller interlayer energies (−90.4 kJ/mol) than intralayer energies (−140.8 kJ/mol) imply that (100) sliding plane is also energetically feasible. For INA form **V**, within the (011) plane identified by Eatt molecules are interconnected through N–H···O (2.94(2) Å) hydrogen bonds, whereas weak interactions C–H···O (3.35(2) Å; 3.37(3) Å) present between layers (Fig. S3). Therefore, the molecules stacking across (011) plane exhibit slightly weaker interaction energy (−113.4 kJ/mol) than the bonding energy within (011) plane (−121.2 kJ/mol), demonstrating comparable intra and interlayer intermolecular bonding energies. It indicated that interlayer energies of INA polymorphs decreased following the order of form **I** > form **II** > form **V** corresponding to the plasticity increased in the order of form **I** > form **II** > form **V** based on a Wang's previous study [36]. Additionally, the other three polymorphs of INA (**III**, **IV** and **IV**) may present plastic property if they could be prepared successfully according to the slip planes and energy calculation results (Tables S4-S6 and Figs. S5-S8 in Supporting information).

Table 1
Total absolute intermolecular interaction energies between the intralayer and interlayer in the slip planes of three isonicotinamide polymorphs calculated by energy framework.

Crystal	Energy framework	Intralayer energy (kJ/mol)	Interlayer energy (kJ/mol)
Form **I**	100	−91.8	−86.2
Form **II**	100	−140.8	−90.4
Form **V**	011	−121.2	−113.4

Table 2
Nanoindentation elastic modulus (*E*) and hardness (*H*) on major crystal faces of three isonicotinamide polymorphs.

Crystal	Indented face	Elastic modulus, *E* (Gpa)	Hardness, *H* (Gpa)
Form **I**	100	12.110 ± 0.515	0.278 ± 0.021
Form **II**	100	20.262 ± 0.660	0.498 ± 0.027
Form **V**	100	15.147 ± 2.985	1.026 ± 0.337

Nanoindentation tests were employed to further examine the relationship between interlayer energy and plasticity and to quantify the mechanical properties of INA polymorphs. Since all three polymorphs are plate-like, the nanoindentation is performed on (100) faces of forms **I**, **II** and **V**. The representative load (*P*) *versus* depth (*h*) curve is illustrated in Fig. 3. The high value of h_{max} and the large residual depths are linked to excellent plastic behavior [37]. At a peak load of 5 mN, the maximum depth of penetration (h_{max}) increased in the order of form **I** (~568 nm) > form **II** (~529 nm) > form **V** (~236 nm), confirming the highest plasticity of form **I**. The elastic modulus (*E*) and nanohardness (*H*) was then estimated from *P-h* response using the standard Oliver-Pharr method [38]. H values of polymorphs decreased in the order of form **I** > form **II** > form **V** (Table 2). Since H reflects the resistance to plastic deformation, the very smallest H value indicates that INA form **I** exhibits the best bending properties [10,39]. From *P-h* curves, forms **I** and **V** indented in (100) faces are comparably smooth, probably due to the presence of parallel slip planes that readily accommodate the advance of indenter tip through facile

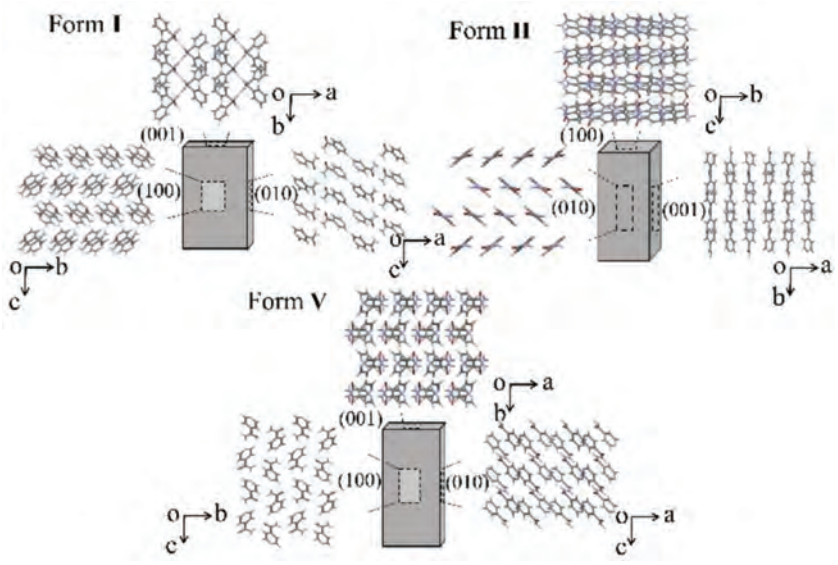

Fig. 2. Molecular packing in forms **I, II** and **V** viewed along (100), (010) and (001) faces.

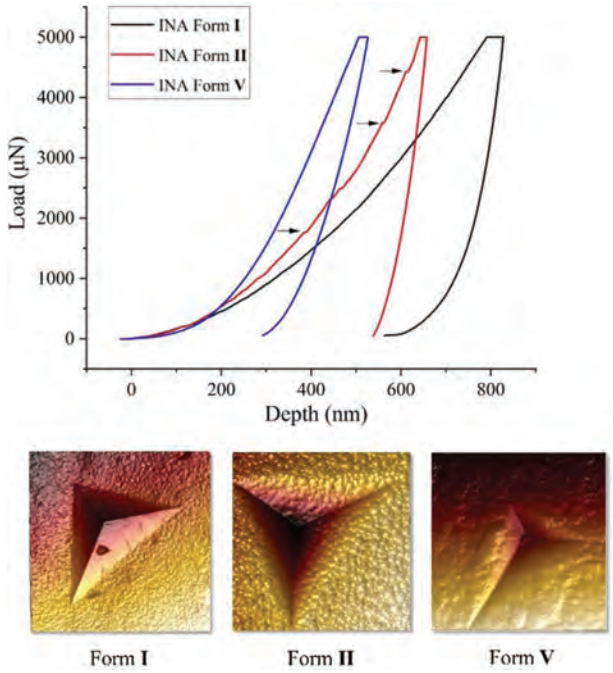

Fig. 3. Representative load–depth (P– h) curves obtained from nanoindentation on (100) faces of forms **I** (black), **II** (red) and **V** (blue) crystals and arrows in form **II** curve indicate the "pop-in" events during loading. AFM diagrams of forms **I, II** and **V**.

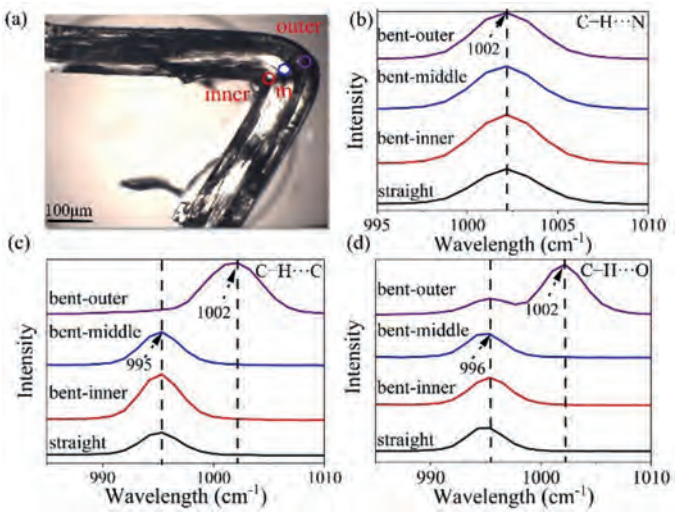

Fig. 4. The microscopic images of the bent crystal and the area for the micro-Raman test in (a) and Raman spectra of straight and deformed crystals of forms **I** (b), **II** (c) and **V** (d).

slip page [18]. Meanwhile, several pop-ins were observed in (100) face of form **II** with the largest elastic modulus value. Pop-ins here can be attributed to sudden stress release when the elastic limit is exceeded and discrete plastic displacement bursts to facilitate easier stress dissipation during indenter tip penetration [40,41]. Verified by nanoindentation experiment, plastic properties of INA forms increased in the order of form **I** > form **II** > form **V**, consistent with decreased order of interlayer energies of INA polymorphs calculated from energy framework. Accordingly, form **I** exhibits the best plasticity among other polymorphs with the weakest interlayer bonding energies.

Micro-Raman spectra were conducted to gain insights into structural changes of bending at the molecular level [18,42]. Raman peak between 970 and 1010 cm^{-1} is the ring breathing mode of pyridine, including ring vibrations and ring bond stretching [43]. Forms **II** and **V** provide a peak at 995–996 cm^{-1} while form **I** shows a peak maximum at 1002 cm^{-1}. The same 995–996 cm^{-1} band in the outer arc demonstrates a blue shift with a broadening of up to 1002 cm^{-1} because of fewer and weaker intermolecular interactions such as C–H···C in form **II** and C–H···O in form **V** produced between pyridine C–H groups and amide groups and carbonyl groups as molecules are farther apart. However, the band of 1002 cm^{-1} in form **I** does not shift from the outer arc to the inner arc due to weak interactions C–H···N formed between pyridine groups that neutralize vibrations and bond stretching of the single pyridine ring when molecules expand (Fig. 4). Thus, bending leads to significant changes in C–H···C, C–H···O, and C–H···N intermolecular weak interactions of the three INA forms.

Additionally, the band at 1611 cm^{-1} is ascribed to stretching vibration of amide N–H groups involved in forming hydrogen-bonded N–H···O and N–H···N and weak interactions C–H···N with carbonyl groups and pyridine groups. The peak intensity at 1611

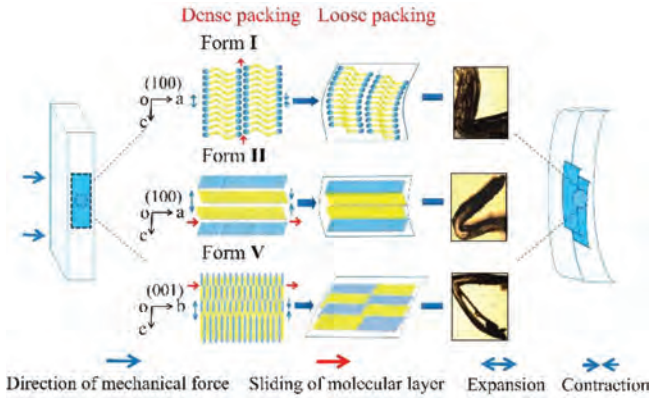

Fig. 5. Plastic bending model of single crystals of INA forms **I** (a), **II** (b) and **V** (c).

cm^{-1} increased in the order of outer > inner > middle > straight, implying that the increase in peak intensity corresponds to a larger intermolecular distance in bent crystal. The shorter distance in the inner arc, when contraction occurs, and longer distance in the outer arc, when expansion occurs [18]. Concurrently, we stated that the intensity of the middle region is the smallest among the other two mentioned above, implying that during crystal bending the molecules in the middle accumulated the most with the closest distance when subjected to compression and tension forces (Figs. S9-S11 in Supporting information).

A schematic depiction of these events is displayed in Fig. 5. The pyridine rings in form **I** are shown as blue balls, and N—H···O hydrogen bonds form between -$CONH_2$ groups represented by yellow right angle disks. They are connected in pairs and extend along *c* axis to produce a column-like structure in form **I** as viewed on the (100) face. The molecules formed in different directions are exhibited by blue and yellow disks, and they are stacked along *c* axis *via* N—H···O hydrogen bonds to generate column-like structure in form **II** on (100) face, while along *b* and *c* axes *via* N—H···O and N—H···N hydrogen bonds, they form zigzag tapes in form **V** on (010) face. Additionally, the white region between columns and tapes corresponds to C—H···N, C—H···C and C—H···O weak interactions, respectively. In short, the bending models depicted in Fig. 5 are composed of columns and tapes, which were stabilized *via* strong hydrogen bonds and weaker interactions in the orthogonal direction. Weaker interactions play a lubricating role between these columns and tapes, thus forming slip planes parallel to the bending face. When subjected to stress, columns can slide more easily than classical stacking flat sheets structure of plastic crystals [44]. Therefore, forms **I** and **II** composed of columns or chains are easy to slide and exhibit better plasticity than form **V**. Although forms **I** and **II** are both composed of columnar structures, the difference of pyridine ring orientation with two-independent 2D tapes to form a column-like structure in form **II** is responsible for less favorable bending geometry of form **II** than form **I** [26]. In addition, molecules in chains or tapes staggered in arrangement make some short-range movements to adapt the bending process, in which the intermolecular distance become longer in the outer arc as molecules stretch and closer in the inner arc as molecules gather. As a result, the bulk crystal demonstrates plastic bending rather than brittle behavior.

The crystal packing of pyrazine-2-carboxamide [13] form I does conform to this bending model with stronger interactions, in which amide dimers are stacked along the *c* axis (3.72 Å) and weak N–H···N (2.46 Å), C–H···O (2.49 Å) and C–H···N (2.55 Å) interactions are present in the other two orthogonal directions and it could be bent under stress (Fig. S12 in Supporting information). While the crystal structure of nicotinamide, with the same molecular weight but different positions of nitrogen atom on pyridine ring, does not conform to the bending model with three-dimensional networks of hydrogen bonds having comparable interactions, this may resist deformation and makes it as a stiff material exhibiting brittle fracture under compressive stress (Fig. S13 in Supporting information) [45].

In conclusion, three INA polymorphs exhibited significant bending properties. The crystal packing with strong and weak interactions in the orthogonal direction of the slip plane is a prerequisite for crystals to exhibit bending mechanical behavior. The super plasticity of INA makes it a good cocrystal coformer to regulate the mechanical behavior of API with poor tabletability. It is a thriving field of chemical material sciences with extensive application prospect.

Declaration of competing interest

The authors declare no conflict of interest.

Acknowledgments

This work was sponsored by National Key R&D Program of China (No. 2016YFC1000900), National Science and Technology Major Project of China (No. 2018ZX09711001–001–013), National Natural Science Foundation of China (No. 81703438).

References

[1] Z. Lu, Y. Zhang, H. Liu, et al., Angew. Chem. Int. Ed. 59 (2020) 4299–4303.
[2] H. Liu, Z. Lu, B. Tang, et al., Angew. Chem. Int. Ed. 59 (2020) 12944–12950.
[3] S. Lv, D.M. Dudek, Y. Cao, et al., Nature 465 (2010) 69–73.
[4] H. Wang, Q. Tang, X. Zhao, et al., ACS Appl. Mater. Interfaces 10 (2018) 2785–2792.
[5] A. Worthy, A. Grosjean, M.C. Pfrunder, et al., Nat. Chem. 10 (2018) 65–69.
[6] E.M. Horstman, R.K. Keswani, B.A. Frey, et al., Angew. Chem. Int. Ed. 56 (2017) 1815–1819.
[7] S. Saha, G.R. Desiraju, J. Am. Chem. Soc. 139 (2017) 1975–1983.
[8] S. Hu, M.K. Mishra, C.C. Sun, Chem. Mater. 31 (2019) 3818–3822.
[9] S. Saha, M.K. Mishra, C.M. Reddy, et al., Acc. Chem. Res. 51 (2018) 2957–2967.
[10] M.K. Mishra, U. Ramamurty, G.R. Desiraju, Curr. Opin. Solid State Mater. Sci. 20 (2016) 361–370.
[11] P. Naumov, S. Chizhik, M.K. Panda, et al., Chem. Rev. 115 (2015) 12440–12490.
[12] C.M. Reddy, M.T. Kirchner, R.C. Gundakaram, et al., Chem. Eur. J. 12 (2006) 2222–2234.
[13] C.M. Reddy, K.A. Padmanabhan, G.R. Desiraju, Cryst. Growth Des. 6 (2006) 2720–2731.
[14] N. Kamali, K. Gniado, P. McArdle, et al., Org. Process Res. Dev. 22 (2018) 796–802.
[15] P. Gupta, S. Allu, D.P. Karothu, et al., Cryst. Growth Des. 21 (2021) 1931–1938.
[16] S. Saha, G.R. Desiraju, Chemistry (Easton) 23 (2017) 4936–4943.
[17] G.R. Krishna, R. Devarapalli, G. Lal, et al., J. Am. Chem. Soc. 138 (2016) 13561–13567.
[18] K. Zhang, C.C. Sun, Y. Liu, et al., Chem. Mater. 33 (2021) 1053–1060.
[19] P. Stainton, T. Grecu, J. McCabe, et al., Cryst. Growth Des. 18 (2018) 4150–4159.
[20] N.B. Báthori, A. Lemmerer, G.A. Venter, et al., Cryst. Growth Des. 11 (2011) 75–87.
[21] J. Seliger, V. Žagar, J. Phys. Chem. A 114 (2010) 12083–12087.
[22] A.I. Vicatos, M.R. Caira, CrystEngComm 21 (2019) 843–849.
[23] C.B. Aakeröy, A.M. Beatty, B.A. Helfrich, et al., Cryst. Growth Des. 3 (2003) 159–165.
[24] P. Vishweshwar, A. Nangia, V.M. Lynch, Cryst. Growth Des. 3 (2003) 783–790.
[25] C.C. Seaton, A. Parkin, C.C. Wilson, et al., Cryst. Growth Des. 9 (2009) 47–56.
[26] J. Li, S.A. Bourne, M.R. Caira, Chem. Commun. 47 (2011) 1530–1532.
[27] S.A. Kulkarni, E.S. McGarrity, H. Meekes, et al., Chem. Commun. 48 (2012) 4983–4985.
[28] K.S. Eccles, R.E. Deasy, L. Fábián, et al., CrystEngComm 13 (2011) 6923–6925.
[29] C. Wang, C.C. Sun, Cryst. Growth Des. 18 (2018) 1909–1916.
[30] Mahjouba Ben Nasr, Kamel Kaabi, Matthias Zeller, et al., Chin. Chem. Lett. 27 (2016) 896–900.
[31] C.C. Sun, Y.H. Kiang, J. Pharm. Sci. 97 (2008) 3456–3461.
[32] H. Liu, J. Nie, C.H. Stephen, et al., Int. J. Pharm. 601 (2021) 120537.
[33] D. Yang, H. Wang, Q. Liu, et al., Chin. Chem. Lett. 33 (2022) 3207–3211.
[34] P.R. Spackman, M.J. Turner, J.J. McKinnon, et al., J. Appl. Crystallogr. 54 (2021) 1006–1011.
[35] Shaokang Tian, Bowen Shao, Zhiqun Wang, et al., Chin. Chem. Lett. 30 (2019) 1289–1292.

[36] C.M. Reddy, S. Basavoju, G.R. Desiraju, Chem. Comm. (2005) 2439–2441.
[37] C.C. Sun, H. Hou, Cryst. Growth Des. 8 (2008) 1575–1579.
[38] W.C. Oliver, G.M. Pharr, J. Mater. Res. 19 (2004) 3–20.
[39] M.K. Mishra, U. Ramamurty, G.R. Desiraju, J. Am. Chem. Soc. 137 (2015) 1794–1797.
[40] M.K. Mishra, G.R. Desiraju, U. Ramamurty, et al., Angew. Chem. Int. Ed. 53 (2014) 13102–13105.
[41] M.S.R.N. Kiran, S. Varughese, C.M. Reddy, et al., Cryst. Growth Des. 10 (2010) 4650–4655.
[42] K. Wang, M.K. Mishra, C.C. Sun, Chem. Mater. 31 (2019) 1794–1799.
[43] M. Bakiler, O. Bolukbasi, A. Yilmaz, J. Mol. Struct. 826 (2007) 6–16.
[44] S.Y. Chang, C.C. Sun, Mol. Pharm. 14 (2017) 2047–2055.
[45] T.V. Joshi, A.B. Singaraju, H.S. Shah, et al., Cryst. Growth Des. 18 (2018) 5853–5865.